https://doi.org/10.5194/egusphere-2025-5230
Preprint. Discussion started: 21 January 2026

Including the triple isotopic composition of dissolved oxygen in the ocean into the iLOVECLIM model (version 1.1.7): development and evaluation

Emeline Clermont[1,2], Ji-Woong Yang[1,2], Didier M. Roche[1,2,3], and Thomas Extier[4]

[1]Laboratoire des Sciences du Climat et de l'Environnement (LSCE), CEA, CNRS, UVSQ, Université Paris-Saclay, Gif-sur-Yvette, France
[2]Institut Pierre-Simon Laplace (IPSL), Université Versailles Saint-Quentin, Guyancourt, France
[3]Earth and Climate Cluster, Faculty of Sciences, Vrije Universiteit Amsterdam, De Boelelaan 1085, 101 HVAmsterdam, the Netherlands
[4]Univ. Bordeaux, CNRS, Bordeaux INP, EPOC, UMR 5805, 33600 Pessac, France

Correspondence: Emeline Clermont (emeline.clermont@lsce.ipsl.fr)

Abstract. Contributing around half of the oxygen produced on Earth, marine photosynthetic production is one of the main mechanisms for carbon fixation, with a central role in the oxygen cycle. The triple isotopic composition of atmospheric oxygen ($^{17}\Delta$), measured in ice cores, provides a global integrator of past biospheric oxygen fluxes, and by extension carbon fluxes. However, deconvolving the signal of $^{17}\Delta$ requires to isolate the oceanic biosphere productivity ($^{17}\Delta_{\mathrm{ocean}}$). Here, we present the first implementation of $^{17}\Delta_{\mathrm{ocean}}$ in the intermediate-complexity climate model iLOVECLIM. The three main processes controlling $^{17}\Delta_{\mathrm{ocean}}$, i.e. photosynthesis, respiration, and air-sea gas exchange, are explicitly represented and evaluated under preindustrial conditions. Model results show overall good agreement with available measurements, particularly in the Pacific Ocean. In contrast, systematic overestimation is found in the Southern Ocean. At fixed stations, seasonality is reproduced but with underestimated amplitude. These discrepancies mainly reflect challenges in representing remineralization and oxygen minimum zones, and highlight opportunities to refine the representation of primary productivity and vertical mixing. Overall, this new implementation provides the first coupled model framework for simulating $^{17}\Delta_{\mathrm{ocean}}$, both as a diagnostic of biogeochemical processes and as a tool for reconstructing past changes in marine productivity. Extending the implementation to the terrestrial biosphere will further allow reconstruction of the past global biosphere and direct comparison with $^{17}\Delta$ records from ice cores.

1 Introduction

The triple isotopic composition of molecular oxygen (O_2), preserved in polar ice cores, is a tracer of the past global biosphere productivity (Luz et al. (1999)). The triple isotopic composition of tropospheric O_2 reflects two major sources: the global

https://doi.org/10.5194/egusphere-2025-5230
Preprint. Discussion started: 21 January 2026

biosphere and the stratosphere. Biogenic O_2 inherits isotopic composition of the source water and is fractionated in mass-dependent manner during biological and hydrological cycling. Conversely, in the stratosphere, O_2 becomes depleted in heavy isotopes in a mass-independent way during ozone-oxygen cycle and isotopic exchange with CO_2 (e.g., Thiemens et al. (1991); Yung et al. (1991); Marcus (2013)). The triple isotopic composition is commonly reported in capital-delta notation ($^{17}\Delta$) defined as follows (Miller (2002)):

$$^{17}\Delta = \left[\ln\left(1+\frac{\delta^{17}O}{1000}\right) - \lambda \times \ln\left(1+\frac{\delta^{18}O}{1000}\right)\right] \times 1\,000\,000 \quad (1)$$

Where: $\delta^{*}O$ is calculated according to the isotopic ratio of sample (*R) and of the isotopic standard ($^{*}R$std): $\delta^{*}O$ = (*R/*Rstd -1) × 1000, * indicating 17 or 18. The isotopic standard of choice is air O_2 (Luz and Barkan (2005)). Isotopic ratio *R (* = 17 or 18) is computed as the ratio of heavy (rare) isotopologues ($^{17}O^{16}O$ and $^{18}O^{16}O$ here) to the most abundant isotopologues ($^{16}O^{16}O$). Since it is biological processes that generate mass-dependent fractionation, the $\delta^{17}O$ anomaly is established in relation to the triple-isotope slope, i.e. λ = 0.518 (Luz and Barkan (2005)). By definition, $^{17}\Delta$ represents the ^{17}O anomaly from the mass-dependent fractionation, and is only weakly altered by mass-dependent fractionation in the biosphere and hydrosphere, while remaining sensitive to mass-independent fractionation signals. As a consequence, modern air is depleted in $^{17}\Delta$ relative to seawater (VSMOW), reflecting stratospheric influx with depleted $^{17}\Delta$ of O_2. As variations in $^{17}\Delta$ are very small, it is expressed in ppm (1 ppm = 0.001 ‰) relative to air.

Beyond its clear advantage of integrating the global (i.e., terrestrial and marine) biosphere signal, $^{17}\Delta$ has the potential to constrain contributions from terrestrial and marine biosphere, relying on slightly different isotopic signatures (e.g., Bender et al. (1994); Luz et al. (1999); Luz and Barkan (2000); Blunier et al. (2002); Landais et al. (2007)). To do so, biological processes and associated isotopic effects need to be implemented in a three-dimensional Earth System Model (ESM) to assess the $^{17}\Delta$ of O_2 produced in the terrestrial ($^{17}\Delta_{\mathrm{terr}}$) and marine biosphere ($^{17}\Delta_{\mathrm{ocean}}$). Previous studies have employ isotope-enabled dynamic global vegetation models or ESM to evaluate $^{17}\Delta_{\mathrm{terr}}$ under past climate boundary conditions, such as during the Last Glacial Maximum (e.g., Landais et al. (2007); Reutenauer et al. (2015); Extier (2019)).

To better quantify the oceanic contribution to the $^{17}\Delta$ and to understand the underlying processes, various ocean-focused models have been developed, ranging from simple box models to complex ocean circulation models, to simulate and better understand the distribution of dissolved O_2, $\delta^{18}O$–O_2, and $^{17}\Delta_{\mathrm{ocean}}$. A variety of one-dimensional models have been constructed for specific purposes, including: estimating respiratory fractionation factors using a vertical advection model in the deep sea (Kroopnick and Craig (1976)); identifying the factors regulating the $\delta^{18}O$–O_2 in deep waters (Bender (1990); Wurgaft et al. (2022); representing $^{17}\Delta_{\mathrm{ocean}}$ under a stable steady-state (Luz and Barkan (2000); Luz and Barkan (2005); Reuer et al. (2007)); and evaluating the impact of physical processes on $^{17}\Delta_{\mathrm{ocean}}$ (Hendricks et al. (2005); Nicholson et al. (2012); Musan et al. (2023)).Two-dimensional isopycnal models have been used to represent $\delta^{18}O$–O_2 in the mesopelagic ocean (Levine et al. (2009)), or to understand the distribution of $\delta^{18}O$–O_2 and $^{17}\Delta_{\mathrm{ocean}}$ data (Li et al. (2022)). Productivity-based models, such as the Vertically Generalized Productivity Model (VGPM; Behrenfeld and Falkowski (1997)) and the Carbon based Productivity Model (CbPM; Westberry et al. (2008)), have also been used to estimate $^{17}\Delta_{\mathrm{ocean}}$ (Juranek and Quay (2010); Munro

https://doi.org/10.5194/egusphere-2025-5230
Preprint. Discussion started: 21 January 2026

et al. (2013)). In order to obtain a more detailed and complex representation, the oxygen isotopes and $^{17}\Delta_{\text{ocean}}$ have been implemented in a global ocean model: the ocean ecosystem and biogeochemistry component of the Community Earth System Model, version 1.1.1. (Nicholson et al. (2014); Palevsky et al. (2016)). However, $^{17}\Delta_{\text{ocean}}$ is not yet implemented in a fully coupled ESM.

All these studies have greatly improved our understanding of these tracers. Both δ^{18}O–O_2 and $^{17}\Delta_{\text{ocean}}$ are governed by three main processes: photosynthesis, respiration and exchange at the ocean-atmosphere interface (Hendricks et al. (2004)). These studies also highlighted several potential biases affecting the interpretation of $^{17}\Delta_{\text{ocean}}$, such as the effect of ocean circulation and the physical processes, or the uncertainties in fractionation coefficients. In order to understand all the processes affecting the triple isotopic composition of dissolved oceanic oxygen, we propose to integrate this tracer into the iLOVECLIM intermediate complexity coupled climate model. This study is divided in three parts: (1) development and verification, (2) evaluation of the model seasonality, (3) evaluation of the minimum oxygen zone representation.

2 Methods

2.1 Oxygen isotopes systematics in the ocean

The calculation of $^{17}\Delta_{\text{ocean}}$ relies on the isotopic composition of dissolved oxygen ($^{32}O_2$, $^{33}O_2$, $^{34}O_2$), which is controlled by three main processes: photosynthesis, respiration, and air-sea gas exchange. Consequently, all these processes must be considered to accurately represent the $^{17}\Delta_{\text{ocean}}$ (Fig. 1 – Green part).

2.1.1 Photosynthesis

Photosynthesis is the primary source of molecular oxygen in the ocean. During this process, the isotopic composition of the O_2 produced can be expressed by partitioning Gross Primary Productivity of Oxygen ($GPPO_2$) among $^{32}O_2$, $^{33}O_2$, $^{34}O_2$:

$$^{*}O_2 \text{ produced} = {}^{*}\alpha_{\text{photosynthesis}} \times {}^{*}R_{\text{SMOW}} \times \frac{GPPO_2}{1 + {}^{17}R_{\text{SMOW}} + {}^{18}R_{\text{SMOW}}} \quad (2)$$

$$^{32}O_2 \text{ produced} = \text{GPPO}_2 - {}^{33}O_2 \text{ produced} - {}^{34}O_2 \text{ produced} \quad (3)$$

Where: $^{*}R_{SMOW}$ denotes the standard isotopic ratio, either ^{17}O/^{16}O (for $^{33}O_2$) or ^{18}O/^{16}O (for $^{34}O_2$), based on the Standard Mean Ocean Water (SMOW) reference. $\alpha_{\text{photosynthesis}}$ is the isotopic fractionation factor during photosynthesis. The denominator accounts for the total isotopic composition of molecular oxygen (^{16}O, ^{17}O, and ^{18}O). It normalizes the gross primary productivity of oxygen flux, effectively converting $GPPO_2$ into its $^{32}O_2$-equivalent. This normalization is required because isotopic ratios are conventionally defined relative to ^{16}O. To ensure conservation of total oxygen productivity, the $^{32}O_2$ produced is calculated as the residual.

https://doi.org/10.5194/egusphere-2025-5230
Preprint. Discussion started: 21 January 2026

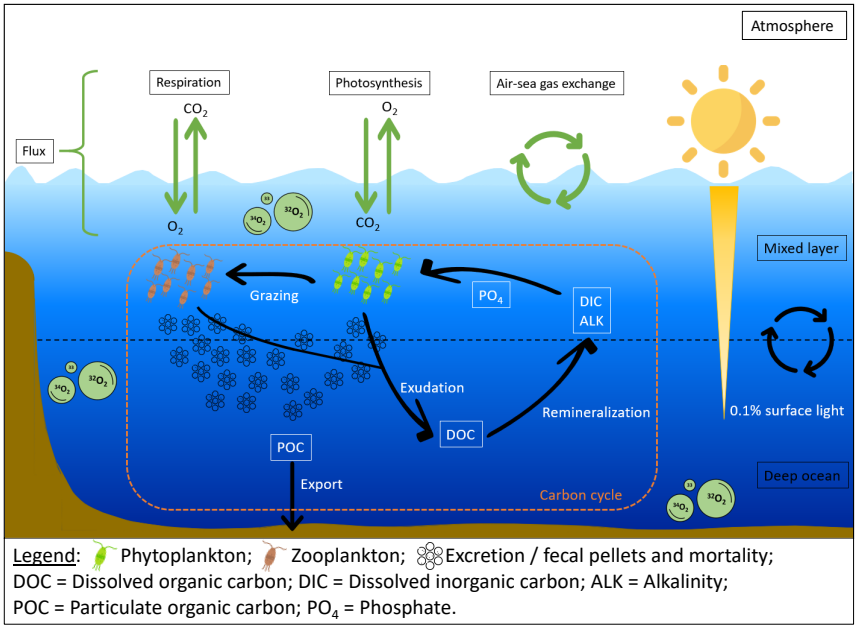

Figure 1. Schematic of the $^{17}\Delta_{\mathrm{ocean}}$ in iLOVECLIM. The orange part determines the carbon cycle. The green section identifies the processes required to implement $^{17}\Delta_{\mathrm{ocean}}$.

2.1.2 Respiration

The oxygen produced by photosynthesis is consumed by the respiration of autotrophic and heterotrophic organisms. Respiration consumes oxygen with a preferential use of light isotopes, generating a mass-dependent fractionation. The $^{17}O/^{16}O$ fractionation factor ($^{17}\alpha_{\mathrm{respiration}}$) is calculated from $^{18}O/^{16}O$ fractionation factor ($^{18}\alpha_{\mathrm{respiration}}$) and the triple isotope fractionation exponent ($^{17/18}\theta$), as follows:

$$^{17}\alpha_{\mathrm{respiration}} = \left(^{18}\alpha_{\mathrm{respiration}}\right)^{^{17/18}\theta} \tag{4}$$

Using the fractionation factors, the respiratory consumption of $^{33}O_2$ and $^{34}O_2$ is computed assuming mass-dependent isotope effects. The respiratory consumption of $^{32}O_2$ is calculated by ensuring isotopic consistency without altering the total oxygen flows in the system:

$$^{*}O_2 \text{ respired} = {}^{*}\alpha_{\mathrm{respiration}} \times {}^{*}R_{O_2} \times \frac{Respiration}{1 + {}^{17}R_{O_2} + {}^{18}R_{O_2}} \tag{5}$$

$$^{32}O_2 \text{ respired} = \text{Respiration} - {}^{33}O_2 \text{ respired} - {}^{34}O_2 \text{ respired} \tag{6}$$

Where: ${}^{*}R_{O_2}$ is the fraction of $^{*}O/^{16}O$ present in the environment. * corresponds to 17 or 18, according to the isotope calculation.

https://doi.org/10.5194/egusphere-2025-5230
Preprint. Discussion started: 21 January 2026

2.1.3 Air-sea gas exchange

To complete the oxygen cycle, exchanges at the air-sea interface must be considered. The net air-sea fluxes of total O_2 is calculated following Nicholson et al. (2012). The negative sign represents that the O_2 molecules are transferred from high to low partial pressure:

$$F_{net} = -k_{O_2}({}^{*}O_{surf} - {}^{*}O_{eq}) \times (1 - f_{ice}) \quad (7)$$

With: Gas piston velocity for oxygen (k_{O_2}), concentration of dissolved O_2 at the surface layer (O_{surf}), saturated concentration of dissolved O_2 (O_{eq}), and ice cover fraction (f_{ice}).

The gas exchange flux of heavy isotopologues is calculated by incorporating both equilibrium (${}^{*}\alpha_{\mathrm{eq}}$) and kinetic isotopic fractionation (${}^{*}\alpha_{\mathrm{k}}$) as follow:

$${}^{*}F = -{}^{*}k_{O_2}[{}^{*}O_{surf} - {}^{*}\alpha_{\mathrm{eq}} \cdot {}^{*}R\mathrm{air} \cdot O\mathrm{eq}/(1 + {}^{17}R\mathrm{air} + {}^{18}R\mathrm{air})] \times (1 - f_{ice}) \quad (8)$$

With: ${}^{*}R_{air}$ is the isotopic ratio of the atmosphere (constant). ${}^{*}O_{surf}$ is the oxygen isotope concentration in the surface layer. The flux of ${}^{32}O_2$ is then calculated as a residual to preserve the total oxygen flux.

2.2 iLOVECLIM model

2.2.1 Presentation

Developed from version 1.2 of the LOVECLIM model (Goosse et al. (2010)), the iLOVECLIM model is a three-dimensional climate model of intermediate complexity. It is based on fluid mechanics equations and operates on a realistic geographical grid. The simplification of the atmospheric physics enables a relatively fast calculation time with 700 to 1000 years per day. iLOVECLIM is undergoing continuous developments integrating various climate tracers, in order to improve the representation of climate processes on different time scales. The model retains the main components of LOVECLIM - atmosphere, ocean and vegetation – as described in Goosse et al. (2010); Roche et al. (2007). Below, we briefly describe only the components essential for representing ${}^{17}\Delta_{\mathrm{ocean}}$: the atmosphere, the ocean, and the ocean carbon cycle (Fig. 1).

The atmospheric component, called ECBilt, is represented by a quasi-geostrophic approach with a T21 spectral grid (resolution of 5.6° in latitude and longitude). The atmosphere is subdivided into three vertical levels, with the mid-point of each layer at 800 hPa, 500 hPa and 200 hPa (Opsteegh et al. (1998)). Humidity is calculated only in the lowest level and is representative of the total humidity content of the atmosphere. Temperature is calculated for two intermediate levels at 650 hPa and 350 hPa. This component represents the entire water cycle (evaporation, precipitation and condensation).

The ocean general circulation component, known as CLIO, is based on the Navier-Stokes equations. Coupled thermodynamically with sea ice (Goosse and Fichefet (1999); Goosse et al. (2010)), this model has a 3×3° horizontal resolution, a vertical

https://doi.org/10.5194/egusphere-2025-5230
Preprint. Discussion started: 21 January 2026

discretization of 20 levels and a free surface that makes it possible to take into account the freshwater input from melting glaciers. Surface temperature and salinity are calculated once a day.

Essential for representing the biological marine ecosystem, the iLOVECLIM model integrates the carbon cycle in the ocean (Bouttes et al. (2015)) based on the equations in Six and Maier-Reimer (1996). This simplified model incorporates a single species of phytoplankton, a single species of zooplankton and a single nutrient, phosphate. Nitrate is derived from phosphate in proportion to Redfield ratios, while iron is not represented in the model. Tracers are transported through the ocean by an diffusion-advection scheme. Following a fitted exponential curve, the remineralization profile is reduced at the surface and accentuated in the deep ocean (Bouttes et al. (2015)).

In this study, the iLOVECLIM model is run under pre-industrial climate boundary conditions, until prognostic variables in the deep ocean reach equilibrium (3,000 years). For these simulations, the following boundary conditions are prescribed: atmospheric CO_2 concentration is fixed at 280 ppm, CH_4 at 760 ppb and N_2O at 270 ppb (Loulergue et al. (2008), Schilt et al. (2010), Bereiter et al. (2015)). The solar constant is maintained at 1365 W m^{-2} throughout the simulation, and the orbital configuration is set according to Berger (1978). Topography, ice sheets and ocean-continent configuration are prescribed according to current observations. The prescribed boundary conditions are consistent with the PMIP standard for pre-industrial (PI) experiments. Model outputs are reported as the annual average of the variable for each pixel, computed over the last 100 years of the simulation.

2.2.2 Implementation of dissolved oxygen

To simulate $^{17}\Delta_{\mathrm{ocean}}$, three tracers representing $^{32}O_2$, $^{33}O_2$ and $^{34}O_2$ are incorporated into iLOVECLIM through previously listed processes (Fig. 1). Their representation follows the framework outlined in Section 2.1. In practice, carbon fluxes in the model are converted into oxygen fluxes using a Redfield ratio, from which the oxygen isotope fluxes are subsequently derived.

The carbon and oxygen cycles are interconnected by biogeochemical processes of photosynthesis and respiration, which involve exchanges between carbon dioxide (CO_2) and oxygen (O_2). Through these processes, a dynamic balance is maintained within the biosphere. In the model, oxygen fluxes are not computed directly but are inferred from carbon fluxes using a Redfield ratio. The total oxygen concentration in the photic zone is thus calculated as the net result of carbon-related biological processes that either produce or consume oxygen. This oxygen balance is called Net Community Production (NCP), and it is defined by the following equation:

$$\mathrm{NCP} = \mathrm{PP} - (P_{\mathrm{remin}} + Z_{\mathrm{remin}}) - \mathrm{DOC} - \mathrm{DOCs} \tag{9}$$

Where: PP is the total phytoplankton production. P_{remin} and Z_{remin} are the fraction of phytoplankton and zooplankton that are remineralized. DOC is Dissolved Organic Carbon. DOCS is the slowly degradable fraction of DOC. Among these terms, only PP results in net oxygen production.

Although NCP represents the net oxygen balance, isotopic calculations require an explicit separation of gross primary productivity of oxygen and respiration. A balanced system is assumed, with $GPPO_2$ defined as twice the total phytoplankton

https://doi.org/10.5194/egusphere-2025-5230
Preprint. Discussion started: 21 January 2026

production, converted into oxygen units using the Redfield ratio. Hence, $GPPO_2$ is calculated using a factor of 2.6, corresponding to the product of the photosynthetic quotient and the Redfield ratio. This factor is close to the ratio between PP (measured by the ^{14}C method) and $GPPO_2$, which is 2.7 according to Marra (2002). Note that this factor can vary from 1.8 to 4.5 depending on the location in the ocean (Juranek and Quay (2013)).

$$GPPO_2 = 2 \times PP \tag{10}$$

Since we cannot distinguish between the autotrophic and heterotrophic respiration in iLOVECLIM, we defined the respiration in a way that conserves the original oxygen budget. As a result, the total respiration of organisms in the mixed layer is defined as:

$$\text{Respiration} = GPPO_2 - NCP \tag{11}$$

While photosynthesis ceases below the photic zone, oxygen consumption can continue down to several kilometers depth, as long as organic matter is available. Respiration is particularly intense in the mesopelagic zone (200–1000 m), where sinking organic matter is actively remineralized. Below this zone, respiration and other oxygen-consuming processes gradually decline with depth. Thus, in the model, these subsurface oxygen consumption processes are represented as:

$$\text{Remineralization} = -DOC - DOCs - POC \tag{12}$$

Where: POC the Particulate Organic Carbon. All terms expressed in carbon units are converted to oxygen units using the Redfield ratio. The remineralization term is negative, as it represents a net consumption of oxygen. Oxygen isotopologues are calculated using the remineralization flux as the consumption term (Section 2.1.2).

In the model, net air-sea fluxes are calculated using a piston velocity parameterized as a quadratic function of wind speed squared (Wanninkhof (1992)), with the oxygen Schmidt number taken from Keeling et al. (1998). The equilibrium saturated oxygen concentration is determined from surface temperature and salinity. Furthermore, for oxygen isotopologues, isotopic fractionations are prescribed as constants. Photosynthesis is implemented without isotopic fractionation ($\alpha_{\text{photosynthesis}}$ = 1). Respiration applies an $^{18}O/^{16}O$ fractionation factor equal to 0.980, with a $^{17/18}\theta$ of 0.518 (Nicholson et al. (2012); Nicholson et al. (2014)). These values can vary depending on environmental conditions, as observed in different studies and experimental measurements (Table 1). Air–sea exchanges consider both equilibrium fractionation and kinetic fractionation, which is defined as Nicholson et al. (2012). To approach the equilibrium values, it should also be noted that the the model is initialized to reproduce a $^{17}\Delta_{\text{ocean}}$ of 41.5 ppm and a $\delta^{18}O$–O_2 of 0.151 ‰. To do this, total dissolved oxygen is set to exactly 250 μmol kg^{-1} and respective isotopic concentrations of $^{32}O_2$ at 249.392 μmol kg^{-1}, $^{33}O_2$ at 0.0959 μmol kg^{-1} and $^{34}O_2$ at 0.5121 μmol kg^{-1}.

https://doi.org/10.5194/egusphere-2025-5230
Preprint. Discussion started: 21 January 2026

Table 1. Respiratory fractionation factors and theta values for ^{17}O and ^{18}O oxygen isotopologues.

	$^{18}\alpha_{respiration}$	Location	$^{17/18}\theta$
Mixed layer	$0.979^{(1)}$	-	$0.518^{(13)}$
	$0.978^{(2)}$	North Pacific Ocean	$0.518 \pm 0.001^{(14)}$
	$0.9785^{(3)}$	-	$0.5179 \pm 0.0006^{(15)}$
	$0.978 \pm 0.0006^{(4)}$	Subarctic Pacific	$0.518^{(16)}$
	$0.978 \pm 0.003^{(5)}$	Southern Ocean	$0.520^{(12,17)}$
	$0.979 \pm 0.002^{(6)}$	Pacific Ocean	$0.5214 \pm 0.0004^{(18)}$
	$0.992^{(7)}$	Mesopelagic zone	-
Depth	$[0.982 ; 0.990]^{(8)}$	-	-
	$[0.980 ; 0.988]^{(4)}$	Subarctic Pacific	-
	0.975 or $0.986^{(9)}$	Red Sea	-
Global	$0.982 \pm 0.003^{(10)}$	Freshwater	-
	$0.980 \pm 0.003^{(11)}$	-	-
	0.982 or $0.989^{(12)}$	-	-

Note: $^{18}\alpha_{respiration}$ and $^{17/18}\theta$ are independent parameters; not all studies report both. References : (1) Kroopnick (1975); (2) Bender and Grande (1987); (3) Guy et al. (1993); (4) Quay et al. (1993); (5) Hendricks et al. (2004); (6) Hendricks et al. (2005); (7) Levine et al. (2009); (8) Bender (1990); (9) Wurgaft et al. (2022); (10) Quay et al. (1995); (11) Kiddon et al. (1993); (12) Li et al. (2022); (13) Angert et al. (2003); (14) Helman et al. (2005); (15) Luz and Barkan (2005); (16) Juranek and Quay (2013); (17) Ash et al. (2020); (18) Sutherland et al. (2022)

2.3 Observational data

To validate the implementation of the $^{17}\Delta_{ocean}$, a total of 2,482 measurements were compiled (Fig. 2). These data were primarily obtained during oceanographic campaigns, where oxygen concentrations were measured either using sensors mounted on a CTD-rosette or by collecting water samples in bottles. The data were processed by averaging replicate measurements and recording their standard deviation. When it was necessary, $^{17}\Delta_{ocean}$ value was recalculated using the logarithmic definition (see above), with a reference slope (λ) of 0.518.

To validate the modelled distribution of total dissolved oxygen, we used annual climatological data from the World Ocean Atlas 2023 (WOA23), provided at 1x1° horizontal resolution (Reagan et al. (2023)). The dataset includes 32,506 unique locations with vertical profiles of dissolved oxygen at various depth. To produce spatial maps from this large dataset, the data points were interpolated using linear interpolation.

https://doi.org/10.5194/egusphere-2025-5230
Preprint. Discussion started: 21 January 2026

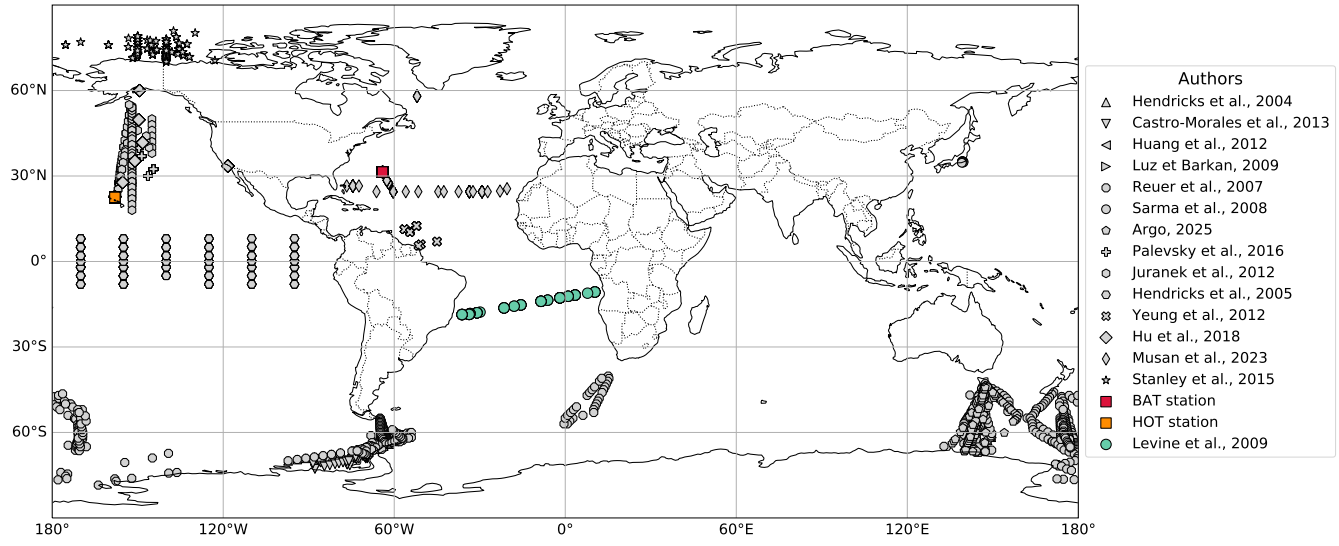

Figure 2. Maps showing measured $^{17}\Delta_{\mathrm{ocean}}$ data. Symbols correspond to datasets of punctual measurements. Green symbols indicate that only δ^{18}O–O_2 measurements are available. Squares indicate continuous measurement stations: BAT and HOT.

3 Results

3.1 Total dissolved oxygen

First, we evaluate the modelled distribution of total dissolved oxygen, which serves as the basis for interpreting oxygen isotope tracers. Since total dissolved oxygen reflects both biogeochemical processes and gas exchanges between the air and the sea, a realistic representation is essential to ensure the robustness of the proxy representation. Overall, the distribution of total dissolved oxygen in the photic zone is generally consistent with the interpolated WOA23 data (Fig. 3). In polar regions, the model exhibits a slight depletion of approximatively 30 μmol kg^{-1} relative to observations. Conversely, some equatorial upwelling areas appear slightly enriched in dissolved oxygen in the model.

Similarly, in the subsurface ocean, the large-scale patterns of dissolved oxygen are generally well captured by the model (Fig. 4). In the Atlantic Ocean, below 2,000 meters, the model tends to underestimate total dissolved oxygen concentrations (Figs. 4b and 4c). In both the Pacific and Atlantic Oceans, Oxygen Minimum Zones (OMZ) are overestimated, with simulated low-oxygen regions extending beyond those observed in the data (Figs. 4a and 4c). In general, the spatial distribution of total dissolved oxygen is reasonably well reproduced by the model, both in the photic zone and at depth, despite some regional discrepancies.

https://doi.org/10.5194/egusphere-2025-5230
Preprint. Discussion started: 21 January 2026

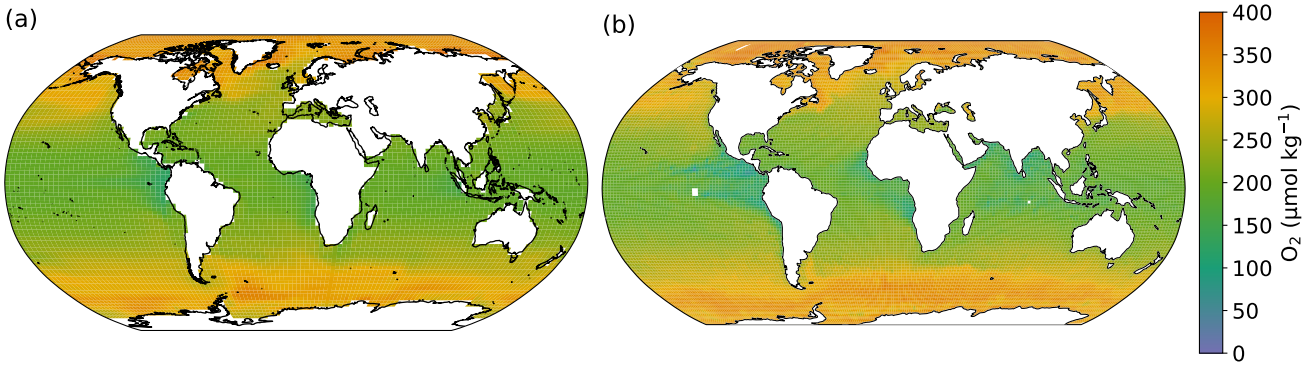

Figure 3. Total dissolved oxygen in the photic layer of the ocean (0-100m). (a) iLOVECLIM. (b) WOA23 database interpolation (Reagan et al. (2023)).

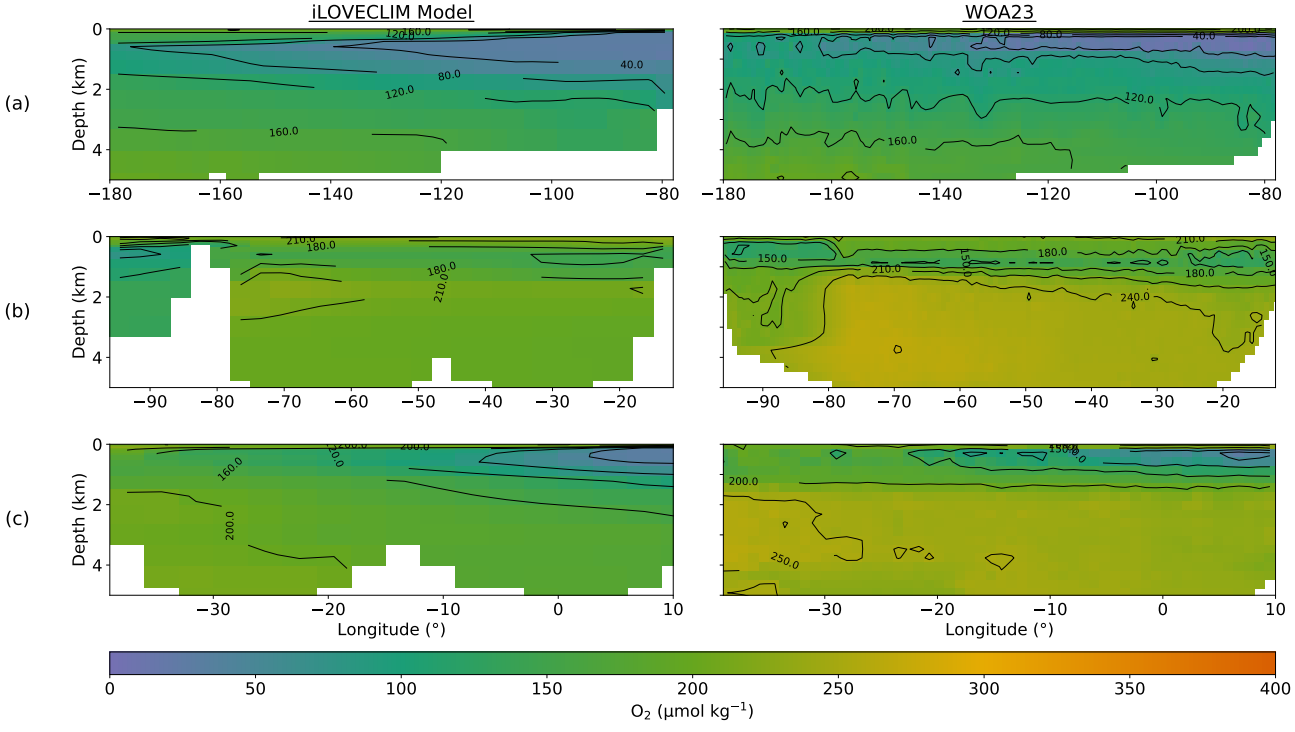

Figure 4. Transects of total dissolved oxygen in the ocean from the iLOVECLIM model (left column) and WOA23 interpolation (right column). Zonal vertical section of meridional mean between (a) 8° S and 5.5° N in Eastern Equatorial Pacific; (b) 24.5 and 28.5° N in the North Atlantic; (c) 10° and 18° S in the tropical South Atlantic Ocean

https://doi.org/10.5194/egusphere-2025-5230
Preprint. Discussion started: 21 January 2026

3.2 Gross primary productivity of oxygen

In the iLOVECLIM mode, the total phytoplankton production is controlled by three parameters: the maximum daily growth rate, which is influenced by sunlight and temperature; the nutrients availability; and the phytoplankton mass (Six and Maier-Reimer (1996)). Since $GPPO_2$ is defined as twice the PP in iLOVECLIM, its spatial distribution is governed by these same processes. After evaluating the model's performance in simulating total dissolved oxygen, we next assess $GPPO_2$, which directly contributes to the isotopic signature observed in surface waters.

Owing to high temperature and maximum solar irradiance, optimum $GPPO_2$ occurs at the equator, reaching 150 mol O_2 m^{-2} d^{-1} (Fig. 5). Upwelling regions, where nutrient supply is enhanced, are also areas of elevated $GPPO_2$. At high latitudes, annual mean $GPPO_2$ remains elevated because intense spring blooms compensate for low winter production. In contrast, at the center of subtropical gyres, $GPPO_2$ is low due to the limited availability of nutrients.

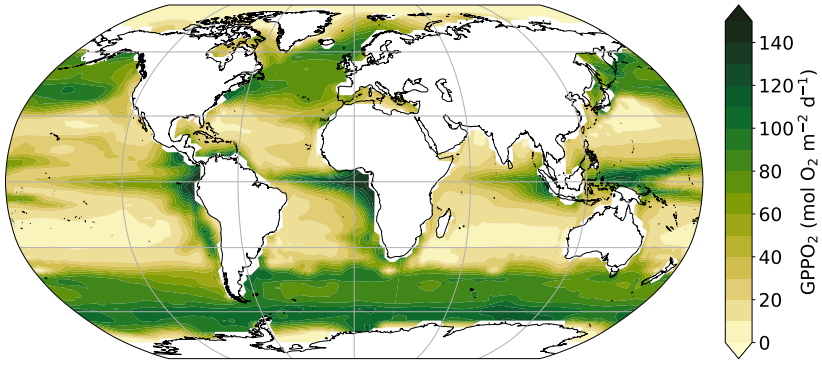

Figure 5. Vertical-integrated $GPPO_2$ distribution in the photic zone (between 0 and 100 meters).

In comparison to the global $GPPO_2$ derived from O_2 measurements during incubation and $^{17}\Delta$ measurements of seawater sample (Huang et al. (2021); Table.2), the $GPPO_2$ is relatively well represented in the model. Consistent with the two calculation methods presented by Huang et al. (2021), global $GPPO_2$ is estimated at 9.68 x 10^{15} mol O_2 yr^{-1} for the pre-industrial simulation (Table.2). However, regional discrepancies are observed: $GPPO_2$ in the Indian Ocean is underestimated, whereas values in the Arctic and the Southern Ocean are overestimated. The underestimation in the Indian Ocean may reflect limitations in the model's representation of regional processes, such as nutrient supply and monsoon-driven dynamics. Conversely, the overestimation at high latitudes may be due to the absence of iron limitation in the model. Iron is a limiting nutrient for phytoplankton growth, especially in high-nutrient low-chlorophyll regions (HNLC), such as the Southern Ocean and parts of the Pacific Ocean.

https://doi.org/10.5194/egusphere-2025-5230
Preprint. Discussion started: 21 January 2026

Table 2. $GPPO_2$ ($\times 10^{15}$ mol O_2 yr^{-1}) in the photic zone of each basin. $GPPO_{2_{LD}}$ and $GPPO_{2_{17\Delta}}$ come from Huang et al. (2021), with $GPPO_2$ estimates by training machine learning and after correction. $GPPO_{2_{LD}}$ is based on O_2 evolution during light-dark bottle incubation. $GPPO_{2_{17\Delta}}$ is based on in situ estimation of $^{17}\Delta_{\mathrm{ocean}}$.

	$GPPO_{2_{\mathrm{iLOVECLIM}}}$	$GPPO_{2_{LD}}$	$GPPO_{2_{17\Delta}}$
Atlantic Ocean	2.49	2.1–3.02	1.75–2.29
Pacific Ocean	3.47	3.92–5.74	3.01–5.57
Indian Ocean	1.08	1.83–2.89	1.53–2.80
Arctic Ocean	0.42	0.18–0.19	0.15–0.18
Southern Ocean	2.16	1.09–2.10	0.90–2.03
Global	9.68	9.5–12.6	7.9–12.2

3.3 Isotopic tracers: δ^{18}O–O_2 and $^{17}\Delta_{\mathrm{ocean}}$

With both total dissolved oxygen and $GPPO_2$ reasonably well reproduced by the iLOVECLIM model, we now examine its capacity to simulate oxygen isotope tracers. As mentioned above, the distribution of these tracers is influenced by various processes, including respiration, photosynthesis and air-sea exchange (Hendricks et al. (2004)). Hence, isotopic tracers are related to the distribution of total dissolved oxygen: when total dissolved oxygen decreases, isotopic tracers increase (Fig. 6). The choice of isotopic fractionation values also affects tracers distributions. Rayleigh curves were plotted using different fractionation values to illustrate the impact of fractionation during respiration (Figs. 6 and 7). Model-data comparison indicates that isotopic tracers are well captured by iLOVECLIM, although some discrepancies appear for $^{17}\Delta_{\mathrm{ocean}}$. These deviations reflect differences in the relative influence of the governing processes.

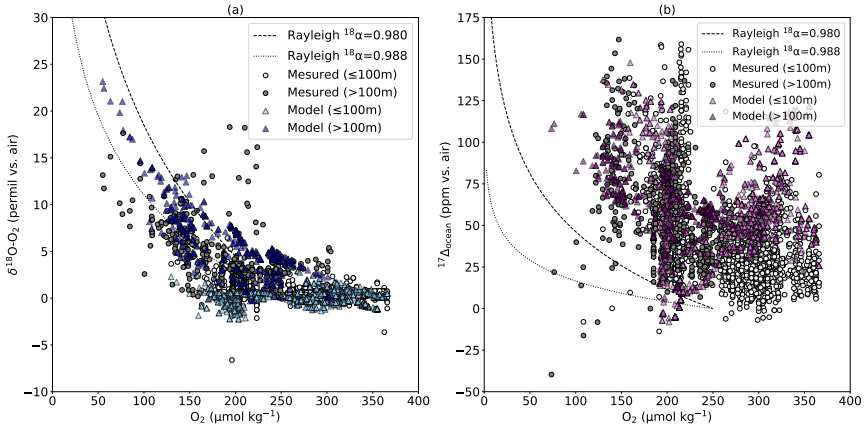

Figure 6. Isotopic tracers according to the total dissolved oxygen concentration. (a) δ^{18}O–O_2. (b) $^{17}\Delta_{\mathrm{ocean}}$. The grey points are the data measurements available (see Fig. 1 for the references). The colored points are the value in the model for the same geographical coordinates as the data. The lines represent Rayleigh slopes with a prescribed alpha.

https://doi.org/10.5194/egusphere-2025-5230
Preprint. Discussion started: 21 January 2026

$\delta^{18}O–O_2$ is primarily affected by respiration (Figs. 6a and 7a). In surface waters, where O_2 is relatively abundant, the combined processes produce a comparatively stable $\delta^{18}O–O_2$ signal. In the subsurface waters, where respiration dominates, $\delta^{18}O–O_2$ follows a Rayleigh-type fractionation trajectory with prescribed fractionation factor. Meanwhile, $^{17}\Delta_{ocean}$ reflects the integrated influence of the three processes (Figs. 6b and 7b). When photosynthesis prevails, both $^{17}\Delta_{ocean}$ and O_2 concentration increase. In both tracers, air–sea gas exchange exerts a restoring effect, driving $\delta^{18}O–O_2$ and $^{17}\Delta_{ocean}$ toward their respective equilibrium values (Fig. 7).

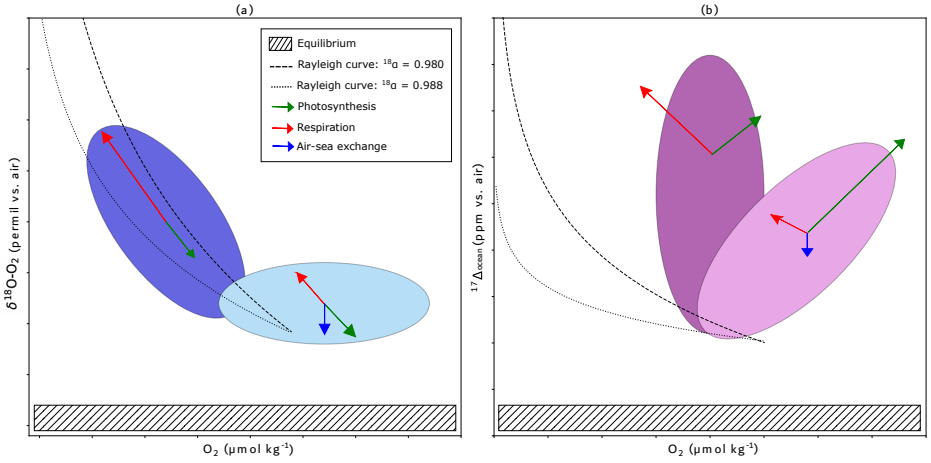

Figure 7. Schematic diagrams of primary factors that control (a) $\delta^{18}O–O_2$ and (b) $^{17}\Delta_{ocean}$ of dissolved O_2. The colored areas show the major distribution of modeled isotopic compositions (Fig. 6). The lighter areas represent the results at the ocean surface, while the darker areas represent the subsurface ocean. Size of arrows qualitatively represent relative contribution of each processes. Axes are not on scale.

The simulated annual mean $\delta^{18}O–O_2$ distribution reveals clear spatial gradients, both at the surface and at depth (Fig. 8). At the surface, $\delta^{18}O–O_2$ is about -0.5 ‰ at the equator, while it is about 1 ‰ at the poles (Fig. 8a). Zones of high productivity (equator, upwelling and Southern Ocean) are marked by a depleted $\delta^{18}O–O_2$, whereas enhanced respiration leads to enrichment. At depth (Figs. 8b and 8c), $\delta^{18}O–O_2$ increases relative to the surface, by an average of 7 ‰ in the Atlantic Ocean and 10 ‰ in the Pacific Ocean. The enriched $\delta^{18}O–O_2$ in the subsurface water masses, in particular around the OMZ, is primarily due to respiration. This is particularly evident within OMZ, where the highest $\delta^{18}O–O_2$ values are observed, reaching ~16‰ in the Atlantic OMZ and up to ~22 ‰ in the Pacific OMZ. The stronger enrichment in the North Pacific compared to the Atlantic reflects the older age of water masses, allowing for greater fractionation along the Rayleigh curve. Deep-ocean $\delta^{18}O–O_2$ values are further modulated by circulation: waters formed in the North Atlantic and around Antarctica begin with relatively high $\delta^{18}O–O_2$, and their progressive aging along circulation pathways enhances enrichment through cumulative respiration.

https://doi.org/10.5194/egusphere-2025-5230
Preprint. Discussion started: 21 January 2026

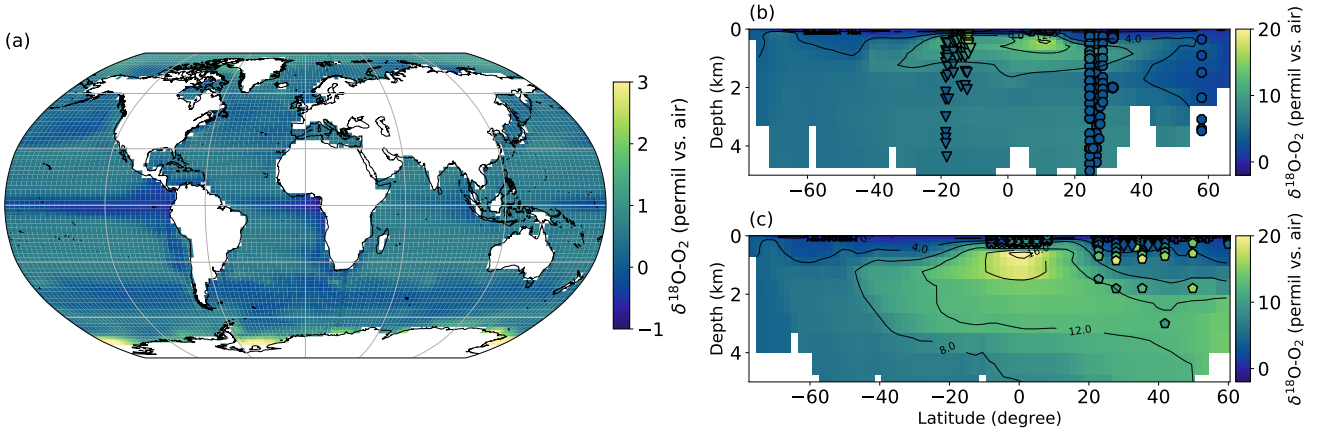

Figure 8. Annual mean distribution of δ^{18}O–O$_2$. Points represent measurements of δ^{18}O–O$_2$ in the ocean from the literature (see Fig. 1 for the references). (a) Surface. (b) N-S cross-section of the central Atlantic Ocean. In this panel, circles represent data from the BAT station, triangles from Levine et al. (2009), hexagons from Luz and Barkan (2005), another set of hexagons from Yeung et al. (2012), octagons from Musan et al. (2023), and stars from Reuer et al. (2007). (c) N-S cross-section of the central Pacific Ocean. In this panel, hexagons represent data from HOT station, crosses from Hendricks et al. (2005), pentagons from Hu et al. (2018), diamonds from Palevsky et al. (2016), stars from Reuer et al. (2007), and plus signs from Juranek and Quay (2013).

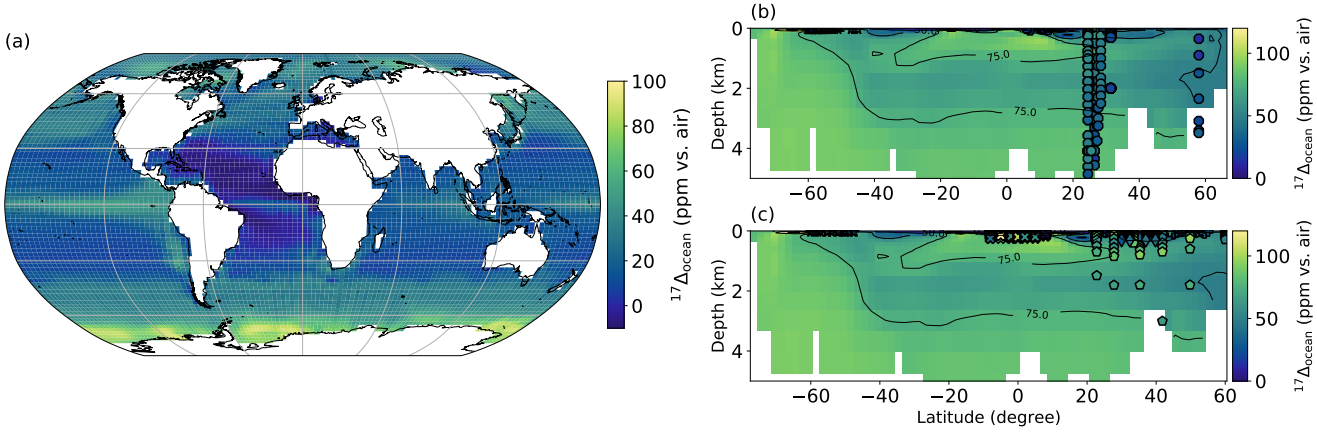

Figure 9. Annual mean distribution of $^{17}\Delta_{\mathrm{ocean}}$. Points represent measurements of $^{17}\Delta_{\mathrm{ocean}}$ in the ocean from the literature (see Fig. 1 for the references). (a) Surface. (b) N-S cross-section of the central Atlantic Ocean. In this panel, circles represent data from the BAT station, hexagons from Luz and Barkan (2005), another set of hexagons from Yeung et al. (2012), octagons from Musan et al. (2023), and stars from Reuer et al. (2007). (c) N-S cross-section of the central Pacific Ocean. In this panel, hexagons represent data from HOT station, crosses from Hendricks et al. (2005), pentagons from Hu et al. (2018), diamonds from Palevsky et al. (2016), stars from Reuer et al. (2007), and plus signs from Juranek and Quay (2013).

https://doi.org/10.5194/egusphere-2025-5230
Preprint. Discussion started: 21 January 2026

The simulated annual mean $^{17}\Delta_{\mathrm{ocean}}$ distribution reveals different spatial gradients as δ^{18}O–O_2 (Fig.9). At the surface, elevated $^{17}\Delta_{\mathrm{ocean}}$ values indicate regions of high productivity, highlighting the dominant role of $GPPO_2$. At the Equator, the $^{17}\Delta_{\mathrm{ocean}}$ is ~50 ppm, compared with -5 to 20 ppm at the center of the ocean gyres (Fig. 9a). In upwelling regions, nutrient input leads to high phytoplankton productivity, with a $^{17}\Delta_{\mathrm{ocean}}$ of around 40 ppm. In polar regions, elevated $^{17}\Delta_{\mathrm{ocean}}$ can be explained by various processes, including the presence of sea ice, or model limitation related to the absence of iron representation. Near Antarctica, values reaching up to 100 ppm are consistent with the seasonal extent of sea ice, which inhibits ocean-atmosphere exchange and leads to the accumulation of $^{17}\Delta_{\mathrm{ocean}}$ beneath the ice. At the end of the Antarctic winter, the maximum extent of sea ice can reach 55° S latitude, emphasizing the vast area where seasonal air–sea fluxes are blocked. At depth, similarly to δ^{18}O–O_2, an increase of $^{17}\Delta_{\mathrm{ocean}}$ values is observed (Figs. 9b and 9c). This vertical distribution can partly be explained by the sinking of water masses, which transports high values to the deep ocean. Additionally, at depth, signals may reflect both the accumulation of respiration and the presence of old water masses.

To reduce the impact of seasonal variability, the model–data comparison focuses on deep-ocean values, where signals are more stable over time (Figs. 8b and 8c, Figs. 9b and 9c). For both δ^{18}O–O_2 and $^{17}\Delta_{\mathrm{ocean}}$, the simulated values fall within the observed range in the Pacific and Atlantic basins. However, in the Atlantic Ocean, modeled values tend to be overestimated in the subsurface ocean. For example, at 20° S and 3 km depth, simulated δ^{18}O–O_2 reach 7 ‰, while observational data indicate a value closer to 3 ‰, corresponding to a relative error of approximatively 133 % (Fig. 8b). At the same location, simulated $^{17}\Delta_{\mathrm{ocean}}$ at 2 km depth shows a relative error of ~30 % compared to observations, with discrepancies increasing below 4 km. Several hypotheses could explain this overestimation, such as: excessive surface oxygen production exported to depth via Antarctic Bottom Water (AABW), or an inaccurate representation of the AABW dynamics in the model. The choice of values for $^{18}\alpha$ and $^{17/18}\theta$ during respiration are also factors that may induce an overestimation. In addition, part of the discrepancy may reflect the inherent uncertainties and sampling limitations of the observational datasets. Musan et al. (2023) suggest that observed data in this region may also be partly influenced by Labrador Sea Water, in particular the Iceland-Scotland Overflow Water (ISOW) and Denmark Strait Overflow Water (DSOW) masses. Such an influence could reduce the apparent discrepancy between simulated and observed $^{17}\Delta_{\mathrm{ocean}}$ values. By contrast, in the model this region is largely dominated by AABW, as illustrated in Fig. 9b.

These results demonstrate that the model provides a robust first-order representation of the $\delta^{18}O$–O2 and $^{17}\Delta ocean$ distributions. The discussion below addresses the origins of the remaining biases.

4 Discussion

4.1 Seasonal effect

The deep ocean results suggest a slight overestimation of $^{17}\Delta_{\mathrm{ocean}}$ driven by AABW formation and water mass sinking. At the surface ocean, away from the equator, the distribution of $^{17}\Delta_{\mathrm{ocean}}$ is additionally modulated by seasonal effects. Therefore, to evaluate its distribution in the photic layer, it is crucial to compare observational data with simulated seasonal $^{17}\Delta_{\mathrm{ocean}}$ outputs. This is particularly relevant given that most of available observational data are measured from surface water samples

https://doi.org/10.5194/egusphere-2025-5230
Preprint. Discussion started: 21 January 2026

collected at specific time, and reflect the state of surface water ecosystem over a few weeks. Year-round observations are only available at research stations (e.g. HOTS, BATS, etc).

For this purpose, monthly modelled $^{17}\Delta_{ocean}$ values were extracted within the photic layer (0-100 m) at the exact locations of the available measurements to allow a direct comparison (Fig. 10). In the Pacific Ocean, simulated $^{17}\Delta_{ocean}$ values generally fall within the observed range. The model performs better during the MAM (March-April-May) and JJA (June-July-August) seasons, while it tends to overestimate values during SON (September-October-November) and DJF (December-January-February) at specific locations. In the Southern Ocean, iLOVECLIM consistently overestimates $^{17}\Delta_{ocean}$, with all simulated points lying above the 1:1 line. Whereas observed values range from 0 to 80 ppm, the model estimates span from 30 to 160 ppm. Notably, neither the data nor the simulations exhibit a clear seasonal pattern. Due to the scarcity of measurements in the Atlantic Ocean, a robust assessment of $^{17}\Delta_{ocean}$ representation in this basin is not possible.

As mentioned above, several hypotheses may explain the overestimation of $^{17}\Delta_{ocean}$ in the Southern Ocean: (1) the absence of iron limitation in the iLOVECLIM model, which favors excessive phytoplankton growth and thus amplifies the photosynthetic $^{17}\Delta_{ocean}$ signal; and/or (2) the accumulation of the $^{17}\Delta_{ocean}$ under sea-ice. However, the second hypothesis is unlikely to play a major role here, as sea ice cover is minimal during the DJF season. Overall, this overestimation is most likely due to an overrepresentation of primary production in the model. Since PP depends on three key parameters, it seems possible to improve its representation by further refining the model and adjusting the parameters.

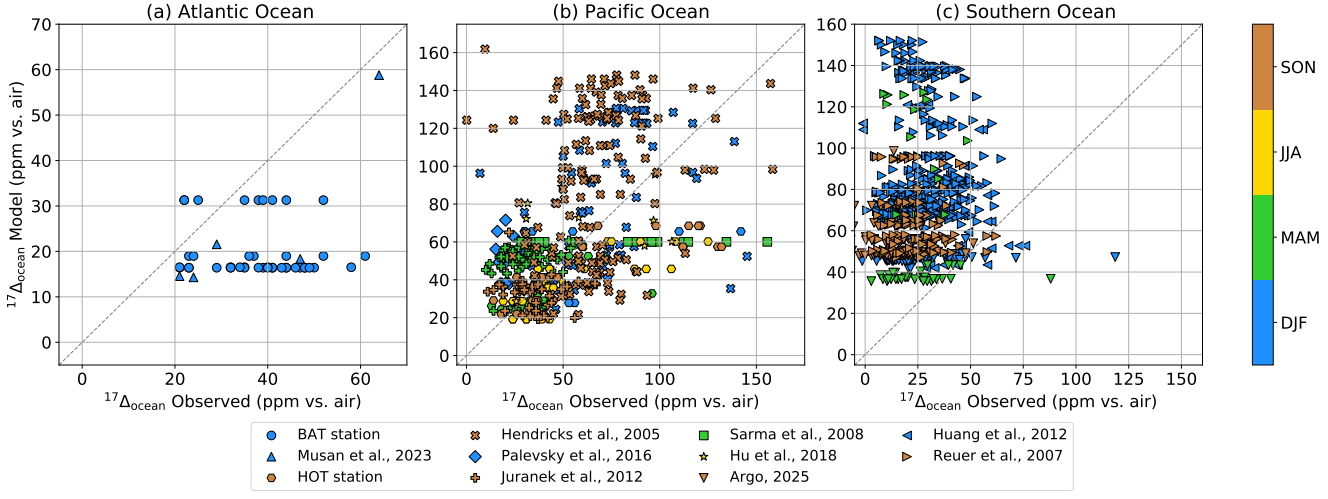

Figure 10. Comparison by basin in the photic zone of simulated $^{17}\Delta_{ocean}$ according to measured $^{17}\Delta_{ocean}$. The different markers represent the references. The colors represent the seasons, with: SON = September, October, November; JJA = June, July, August; MAM = March, April, May; DJF = December, January, February. The black dotted line represents a 1:1 straight line.

https://doi.org/10.5194/egusphere-2025-5230
Preprint. Discussion started: 21 January 2026

Year-round measurements at the BATS and HOTS allow for the seasonal assessment of the model's ability to represent $^{17}\Delta_{ocean}$ across depth and basin at fixed coordinates. Overall, both measured and simulated $^{17}\Delta_{ocean}$ display seasonal variability within the upper photic layer (Fig. 11). At BATS, measured $^{17}\Delta_{ocean}$ stabilizes below 250 m, while at HOTS, stabilization occurs around 300 m across all seasons. In contrast, the modelled $^{17}\Delta_{ocean}$ stabilizes much shallower, around 100 m, limited by the prescribed photic layer depth. In both observational and simulated profiles, the most pronounced seasonal variation occurs between 50 m and 100 m. While the model successfully captures the seasonal trend, it underestimates the amplitude. For instance, during SON, $^{17}\Delta_{ocean}$ peaks at 120 ppm in the measurements, but only reaches 75 ppm in the model. Despite this underestimation, the seasonal cycle of $^{17}\Delta_{ocean}$ in the photic layer is reasonably well reproduced.

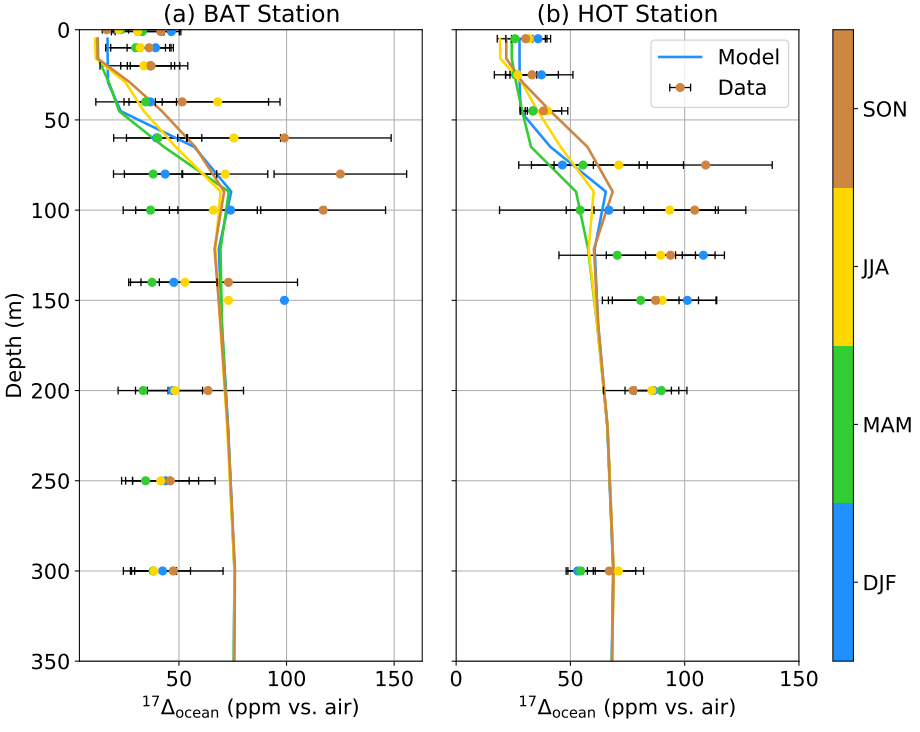

Figure 11. Vertical profile of $^{17}\Delta_{ocean}$ according to the seasons, in Bermuda Atlantic Time-series (BAT) and in Hawaii Ocean Time-series (HOT). The lines represent the simulated evolution of $^{17}\Delta_{ocean}$, while the dots represent measured $^{17}\Delta_{ocean}$ values with associated error bars. The colors represent the seasons, as described in Figure 10.

Overall, the model captures the seasonal trend of $^{17}\Delta_{ocean}$ reasonably well across different spatial scales, from ocean basins to fixed-point stations. However, it systematically over-estimates absolute $^{17}\Delta_{ocean}$ values in the Pacific and Southern Oceans when compared point by point with observations. At station level, although the seasonal phase is reproduced, the amplitude remains underestimated and the vertical structure is too shallow, likely due to limitations in the photic layer depth and primary production representation. Indeed, limited variability in PP can reduce the production of oxygen, leading to an

https://doi.org/10.5194/egusphere-2025-5230
Preprint. Discussion started: 21 January 2026

underestimation of $^{17}\Delta_{\mathrm{ocean}}$ at these stations. Other factors, such as local mixing processes or nutrient limitations, may also contribute, but the insufficient seasonal modulation of biological activity appears to be a primary driver (Appendix A). These discrepancies suggest that while the timing of seasonal variability is well represented, further refinement of the biological and vertical mixing processes in the model is necessary to improve the magnitude and spatial distribution of $^{17}\Delta_{\mathrm{ocean}}$. Importantly, the implementation of $^{17}\Delta_{\mathrm{ocean}}$ revealed this bias, providing a direct diagnostic of the model's ability to reproduce seasonal cycles.

4.2 Oxygen minimum zone

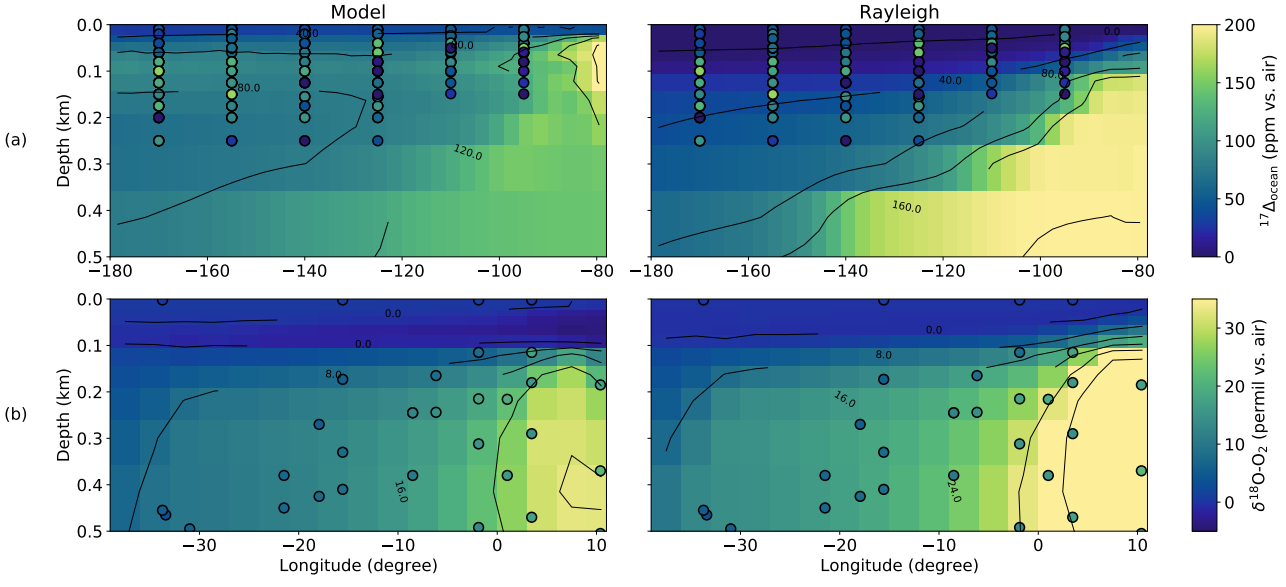

Figure 12. East-west transect of isotopic proxies at depth. The first column "Model" represents the result of the model. The second column "Rayleigh" represents the proxy calculated theoretically according to the Rayleigh slope with $\alpha = 0.980$ (Fig. 6), based on the oxygen present in the model. The dots represent the measured proxy. (a) Zonal vertical section of meridional mean of $^{17}\Delta_{\mathrm{ocean}}$ between 8° S and 5.5° N in Eastern Equatorial Pacific. (b) Zonal vertical section of meridional mean of δ^{18}O–O_2 between 10° and 18° S in the tropical South Atlantic Ocean.

Beyond seasonal dynamics, the distribution of total dissolved oxygen is another factor that can indirectly influence $^{17}\Delta_{\mathrm{ocean}}$. In iLOVECLIM, oxygen minimum zones tend to expand excessively, leading to unrealistic remineralization rates. To prevent such issues, an ad hoc lower oxygen threshold was introduced in the model. After testing, a minimum total oxygen concentration of 30 μmol kg^{-1} was established, below which remineralization is halted to ensure numerical stability. However, this constraint also prevents the full development of OMZ. While it avoids unrealistic anoxia, it limits the emergence of strong subsurface oxygen gradients, which in turn may reduce the biogeochemical contrast necessary to simulate realistic isotopic composition around this region.

https://doi.org/10.5194/egusphere-2025-5230
Preprint. Discussion started: 21 January 2026

To further evaluate the representation of $^{17}\Delta_{\mathrm{ocean}}$ and $\delta^{18}\mathrm{O}$–O_2 in the model, we compare them against the OMZ using both theoretical estimates and available observations (Fig. 12). The theoretical proxy is computed using a Rayleigh fractionation model, which isolates the effect of respiration while neglecting photosynthesis, water mass mixing and air–sea exchange. It provides a useful benchmark to assess the consistency between the simulated oxygen field (Fig. 4) and the expected isotopic gradients, by isolating the influence of remineralization. This comparison serves as a diagnostic of the model's internal consistency.

In the eastern equatorial Pacific, both the model and theoretical calculations show an eastward increase in $^{17}\Delta_{\mathrm{ocean}}$, near the American coast (Fig. 12a). However, sparse observational data in this region limit direct validation. The theoretical signal exhibits a more pronounced vertical gradient and higher values toward the east compared to the model. In contrast, the simulated $^{17}\Delta_{\mathrm{ocean}}$ is further diffuse, potentially due to excessive smoothing of primary production, limited vertical resolution, or inaccurately tuned remineralization rates. Additional contributions may arise from inaccurate isotopic fractionation values during both photosynthesis and respiration, which would directly affect the magnitude and vertical structure of $^{17}\Delta_{\mathrm{ocean}}$. For $\delta^{18}\mathrm{O}$–O_2 (Fig. 12b), the model simulates strong enrichment along the eastern boundary, where OMZ are expected (Fig. 4c). However, observed values are lower, suggesting an overestimation of the isotopic signal associated with respiration. This bias may result from excessive remineralization just above the 30 μmol.kg^{-1} threshold in iLOVECLIM, which suppresses anoxia while still allowing intense localized biogeochemical activity. Other potential biases include excessive remineralization rates, overestimation of isotopic fractionation during respiration, or mixing between different water masses. In addition, limited vertical mixing may amplify this signal. While remineralization under low oxygen conditions could occur, the behavior of isotopic fractionation under such conditions remains largely unknown. Diapycnal mixing may also contribute to the observed patterns. As a result, the model produces a truncated OMZ but an exaggerated isotopic response, complicating the interpretation of $\delta^{18}\mathrm{O}$–O_2 in these regions.

Overall, this comparison highlights the value of combining isotopic proxies, theoretical simulations, and biogeochemical fields to diagnose internal model limitations. In particular, when the oxygen field reproduces expected structures but the associated isotopic signal does not, this may indicate a decoupling between biological processes and isotopic dynamics.

5 Conclusions

In this study, we implemented the triple isotopic composition of dissolved oxygen into the iLOVECLIM model, providing the first representation of $^{17}\Delta_{\mathrm{ocean}}$ in a 3D Earth System Model of intermediate complexity. Validation against available observations shows that total dissolved oxygen, GPPO_2 and $\delta^{18}\mathrm{O}$–O_2 are reasonably well represented, enabling the model to simulate coherent $^{17}\Delta_{\mathrm{ocean}}$ distributions. The model successfully captures the timing of seasonal variability in oxygen isotopes, demonstrating its ability to reproduce large-scale temporal dynamics. However, a key limitation lies in the representation of oxygen minimum zones, which remains constrained by the imposed oxygen threshold. To improve the spatial distribution and magnitude of $^{17}\Delta_{\mathrm{ocean}}$, further refinement of primary production schemes and vertical mixing processes is needed. These findings emphasize the possibility of constantly improving the reproduction of this proxy. They also highlight the importance

https://doi.org/10.5194/egusphere-2025-5230
Preprint. Discussion started: 21 January 2026

of understanding the underlying physical and biogeochemical processes affecting the $^{17}\Delta$. This new implementation also opens the way for future applications of iLOVECLIM to reconstruct past variations in ocean productivity. The future integration of terrestrial $^{17}\Delta_{\mathrm{terr}}$ into iLOVECLIM will also enable the reconstruction of the past global biosphere and the comparison of these reconstructions with $^{17}\Delta$ measurements from air bubbles in ice cores.

Code and data availability. The source code of the iLOVECLIM model used in this study (version 1.1.7) is archived on Zenodo (DOI: https://doi.org/10.5281/zenodo.17379487, Clermont and Roche (2025)). For further information about the code, please contact Didier M. Roche (didier.roche@lsce.ipsl.fr). The model outputs used to generate the oxygen and tracers figures are available on Zenodo (DOI: https://doi.org/10.5281/zenodo.17379193, Clermont (2025)).

Observational data used for model–data comparison were obtained from the cited sources, except for the dataset from Hendricks et al. (2004) and Hendricks et al. (2005). The dataset described in Stanley et al. (2015) is publicly available at: http://www.whoi.edu/beaufortgyre. $^{17}\Delta_{\mathrm{ocean}}$ measurements from the BAT and HOT stations were taken from Nicholson et al. (2012). The dataset described in Argo (2025) and Hu et al. (2018) were analyzed in Bender et al. (2016) and Li et al. (2022), respectively.

https://doi.org/10.5194/egusphere-2025-5230
Preprint. Discussion started: 21 January 2026

Appendix A: Seasonal phytoplankton productivity (PP)

In the main text, we compared the results of $^{17}\Delta_{ocean}$ at the BATS and HOT stations. One possible explanation for the limited variability observed is the relatively stable phytoplankton productivity (PP) in these regions. To explore this further, we compared the model outputs with available PP observations at the BAT (Johnson et al. (2025)) and HOT (White et al. (2025)) stations.

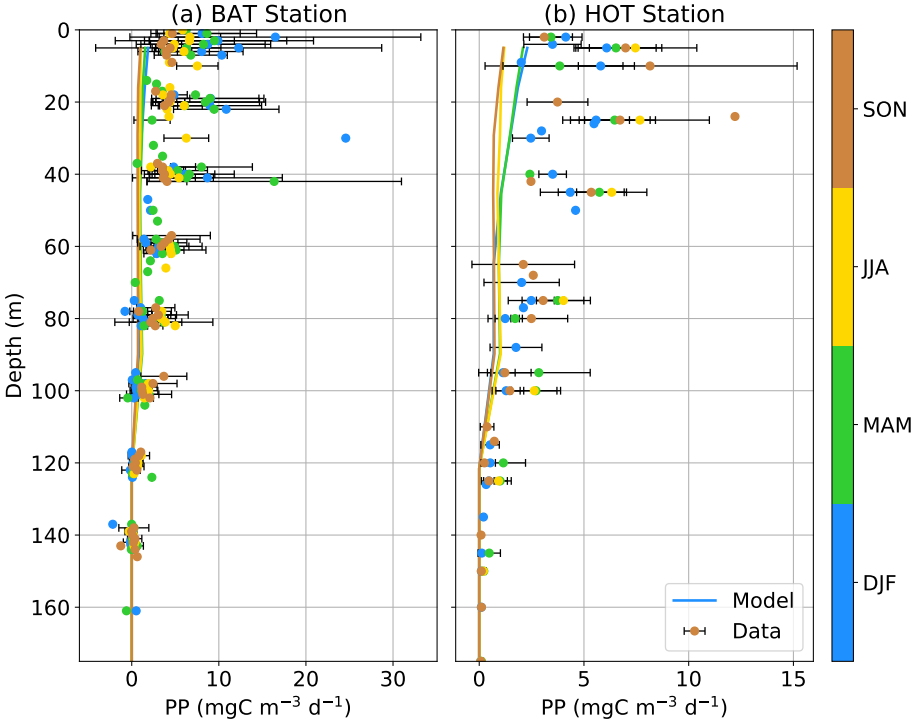

Figure A1. Vertical profile of phytoplankton productivity according to the seasons, in Bermuda Atlantic Time-series (BAT) and in Hawaii Ocean Time-series (HOT). The lines represent the simulated evolution of PP, while the dots represent measured PP values with associated error bars. The colors represent the seasons.

Figure A1 shows that PP exhibits only limited seasonal variability at both sites. This limited variability likely reflects the relatively stable environmental conditions in these subtropical regions. PP is calculated according to three paramters wich are: nutrient availability, temperature and light function, and finally phytoplankton mass. Refining the parameterization of these drivers could help improve the representation of seasonal PP, and consequently, the seasonal behavior of $^{17}\Delta_{ocean}$.

It is worth noting that the model used here is of intermediate complexity. While not all biogeochemical processes are explicitly represented, it provides a robust annual mean representation of $^{17}\Delta_{ocean}$, consistent with the scope and objectives of this study.

https://doi.org/10.5194/egusphere-2025-5230
Preprint. Discussion started: 21 January 2026

Author contributions. EC conducted the study with the help of the co-authors. EC and DMR developed the code. EC analyzed the model results. EC, JWY, TE, and DMR discussed interpretations. EC wrote the manuscript. JWY, TE, and DMR contributed to the writing of the manuscript.

Competing interests. Didier M. Roche is the coordinator of the special issue "The iLOVECLIM earth system model".

Acknowledgements. The authors are grateful to Melissa Hendricks for sharing her dataset fom the equatorial Pacific and the Southern Ocean. This research was funded, in whole or in part, by the Agence Nationale de la Recherche (ANR), grant ANR-22-CPJ1-0081-01, awarded to JWY. EC acknowledges support from the Ministère de l'Enseignement supérieur, de la Recherche et de l'Innovation.

https://doi.org/10.5194/egusphere-2025-5230
Preprint. Discussion started: 21 January 2026

References

Angert, A., Barkan, E., Barnett, B., Brugnoli, E., Davidson, E. A., Fessenden, J., Maneepong, S., Panapitukkul, N., Randerson, J. T., Savage, K., Yakir, D., and Luz, B.: Contribution of soil respiration in tropical, temperate, and boreal forests to the ^{18}O enrichment of atmospheric O_2, Global Biogeochemical Cycles, 17, 2003GB002 056, https://doi.org/10.1029/2003GB002056, 2003.

Argo: Argo float data and metadata from Global Data Assembly Centre (Argo GDAC), https://doi.org/10.17882/42182, 2025.

Ash, J., Hu, H., and Yeung, L.: What fractionates oxygen isotopes during respiration? Insights from multiple isotopologue measurements and theory., ACS Earth and Space Chemistry, 4, 50–66, https://doi.org/https://doi.org/10.1021/acsearthspacechem.9b00230, 2020.

Behrenfeld, M. J. and Falkowski, P. G.: Photosynthetic rates derived from satellite-based chlorophyll concentration, Limnology and Oceanography, 42, 1–20, https://doi.org/10.4319/lo.1997.42.1.0001, 1997.

Bender, M., Sowers, T., and Labeyrie, L.: The Dole Effect and its variations during the last 130,000 years as measured in the Vostok Ice Core, Global Biogeochemical Cycles, 8, 363–376, https://doi.org/10.1029/94GB00724, 1994.

Bender, M. L.: The δ^{18} O of dissolved O_2 in seawater: A unique tracer of circulation and respiration in the deep sea, J. Geophys. Res., 95, 22 243–22 252, https://doi.org/10.1029/JC095iC12p22243, 1990.

Bender, M. L. and Grande, K. D.: Production, respiration, and the isotope geochemistry of O2 in the upper water column, Global Biogeochemical Cycles, 1, 49–59, https://doi.org/10.1029/GB001i001p00049, _eprint: https://agupubs.onlinelibrary.wiley.com/doi/pdf/10.1029/GB001i001p00049, 1987.

Bender, M. L., Tilbrook, B., Cassar, N., Jonsson, B., Poisson, A., and Trull, T. W.: Ocean productivity south of Australia during spring and summer, Deep Sea Research Part I: Oceanographic Research Papers, 112, 68–78, https://doi.org/10.1016/j.dsr.2016.02.018, 2016.

Bereiter, B., Eggleston, S., Schmitt, J., Nehrbass-Ahles, C., Stocker, T. F., Fischer, H., Kipfstuhl, S., and Chappellaz, J.: Revision of the EPICA Dome C CO_2 record from 800 to 600 kyr before present, Geophysical Research Letters, 42, 542–549, https://doi.org/10.1002/2014GL061957, 2015.

Berger, A.: Long-Term Variations of Daily Insolation and Quaternary Climatic Changes, https://journals.ametsoc.org/view/journals/atsc/35/12/1520-0469_1978_035_2362_ltvodi_2_0_co_2.xml, section: Journal of the Atmospheric Sciences, 1978.

Blunier, T., Barnett, B., Bender, M. L., and Hendricks, M. B.: Biological oxygen productivity during the last 60,000 years from triple oxygen isotope measurements, Global Biogeochemical Cycles, 16, https://doi.org/10.1029/2001GB001460, 2002.

Bouttes, N., Roche, D. M., Mariotti, V., and Bopp, L.: Including an ocean carbon cycle model into *i*LOVECLIM (v1.0), Geosci. Model Dev., 8, 1563–1576, https://doi.org/10.5194/gmd-8-1563-2015, 2015.

Castro-Morales, K., Cassar, N., Shoosmith, D. R., and Kaiser, J.: Biological production in the Bellingshausen Sea from oxygen-to-argon ratios and oxygen triple isotopes, Biogeosciences, 10, 2273–2291, https://doi.org/10.5194/bg-10-2273-2013, publisher: Copernicus GmbH, 2013.

Clermont, E.: Model outputs : oxygen, oxygen isotopes and gross primary productivity of oxygen (iLOVECLIM v1.1.7), https://doi.org/10.5281/zenodo.17379193, 2025.

Clermont, E. and Roche, D. M.: iLOVECLIM source code (version 1.1.7), https://doi.org/10.5281/zenodo.17379487, 2025.

Extier, T.: Variations climatiques et variations du cycle hydrologique aux basses latitudes au cours du Quaternaire : une approche combinant modèle et données, phdthesis, Université Paris Saclay (COmUE), https://theses.hal.science/tel-02986449, 2019.

Goosse, H. and Fichefet, T.: Importance of ice-ocean interactions for the global ocean circulation: A model study, J. Geophys. Res., 104, 23 337–23 355, https://doi.org/10.1029/1999JC900215, 1999.

https://doi.org/10.5194/egusphere-2025-5230
Preprint. Discussion started: 21 January 2026

Goosse, H., Brovkin, V., Fichefet, T., Haarsma, R., Huybrechts, P., Jongma, J., Mouchet, A., Selten, F., Barriat, P.-Y., Campin, J.-M., Deleersnijder, E., Driesschaert, E., Goelzer, H., Janssens, I., Loutre, M.-F., Morales Maqueda, M. A., Opsteegh, T., Mathieu, P.-P., Munhoven, G., Pettersson, E. J., Renssen, H., Roche, D. M., Schaeffer, M., Tartinville, B., Timmermann, A., and Weber, S. L.: Description of the Earth system model of intermediate complexity LOVECLIM version 1.2, Geosci. Model Dev., 3, 603–633, https://doi.org/10.5194/gmd-3-603-2010, 2010.

Guy, R. D., Fogel, M. L., and Berry, J. A.: Photosynthetic Fractionation of the Stable Isotopes of Oxygen and Carbon, Plant Physiology, 101, 37–47, https://doi.org/10.1104/pp.101.1.37, _eprint: https://academic.oup.com/plphys/article-pdf/101/1/37/35937875/plphys_v101_1_37.pdf, 1993.

Helman, Y., Barkan, E., Eisenstadt, D., Luz, B., and Kaplan, A.: Fractionation of the Three Stable Oxygen Isotopes by Oxygen-Producing and Oxygen-Consuming Reactions in Photosynthetic Organisms, Plant Physiology, 138, 2292–2298, https://doi.org/10.1104/pp.105.063768, 2005.

Hendricks, M. B., Bender, M. L., and Barnett, B. A.: Net and gross O2 production in the southern ocean from measurements of biological O2 saturation and its triple isotope composition, Deep Sea Research Part I: Oceanographic Research Papers, 51, 1541–1561, https://doi.org/10.1016/j.dsr.2004.06.006, 2004.

Hendricks, M. B., Bender, M. L., Barnett, B. A., Strutton, P., and Chavez, F. P.: Triple oxygen isotope composition of dissolved O_2 in the equatorial Pacific: A tracer of mixing, production, and respiration, J. Geophys. Res., 110, 2004JC002 735, https://doi.org/10.1029/2004JC002735, 2005.

Hu, H., Yeung, L., Berelson, W., and Young, E.: Depth profiles of dissolved O2 saturation and isotopologues from the R/V Yellowfin and R/V Kilo Moana from 2016-09-14 to 2017-08-28., https://doi.org/10.1575/1912/bco-dmo.753594.1, 2018.

Huang, K., Ducklow, H., Vernet, M., Cassar, N., and Bender, M. L.: Export production and its regulating factors in the West Antarctica Peninsula region of the Southern Ocean, Global Biogeochemical Cycles, 26, https://doi.org/10.1029/2010GB004028., 2012.

Huang, Y., Nicholson, D., Huang, B., and Cassar, N.: Global Estimates of Marine Gross Primary Production Based on Machine Learning Upscaling of Field Observations, Global Biogeochemical Cycles, 35, e2020GB006 718, https://doi.org/10.1029/2020GB006718, 2021.

Johnson, R. J., Bates, N., Lethaby, P. J., Smith, D., Medley, C., Stuart, E., and May, R.: Primary productivity estimates from the incubation of seawater collected at the Bermuda Atlantic Time-series Study (BATS) site from December 1988 through December 2024, https://doi.org/10.26008/1912/BCO-DMO.893182.6, 2025.

Juranek, L. and Quay, P.: Using Triple Isotopes of Dissolved Oxygen to Evaluate Global Marine Productivity, Annu. Rev. Mar. Sci., 5, 503–524, https://doi.org/10.1146/annurev-marine-121211-172430, 2013.

Juranek, L. W. and Quay, P. D.: Basin-wide photosynthetic production rates in the subtropical and tropical Pacific Ocean determined from dissolved oxygen isotope ratio measurements, Global Biogeochemical Cycles, 24, 2009GB003 492, https://doi.org/10.1029/2009GB003492, 2010.

Juranek, L. W., Quay, P. D., Feely, R. A., Lockwood, D., Karl, D. M., and Church, M. J.: Biological production in the NE Pacific and its influence on air-sea CO2 flux: Evidence from dissolved oxygen isotopes and O2/Ar, Journal of Geophysical Research: Oceans, 117, https://doi.org/10.1029/2011JC007450, _eprint: https://agupubs.onlinelibrary.wiley.com/doi/pdf/10.1029/2011JC007450, 2012.

Keeling, R. F., Stephens, B. B., Najjar, R. G., Doney, S. C., Archer, D., and Heimann, M.: Seasonal variations in the atmospheric O_2 /N_2 ratio in relation to the kinetics of air-sea gas exchange, Global Biogeochemical Cycles, 12, 141–163, https://doi.org/10.1029/97GB02339, 1998.

https://doi.org/10.5194/egusphere-2025-5230
Preprint. Discussion started: 21 January 2026

Kiddon, J., Bender, M. L., Orchardo, J., Caron, D. A., Goldman, J. C., and Dennett, M.: Isotopic fractionation of oxygen by respiring marine organisms, Global Biogeochemical Cycles, 7, 679–694, https://doi.org/10.1029/93GB01444, 1993.

Kroopnick, P. and Craig, H.: Oxygen isotope fractionation in dissolved oxygen in the deep sea, Earth and Planetary Science Letters, 32, 375–388, https://doi.org/https://doi.org/10.1016/0012-821X(76)90078-9, 1976.

Kroopnick, P. M.: Respiration, photosynthesis, and oxygen isotope fractionation in oceanic surface water1, Limnology & Oceanography, 20, 988–992, https://doi.org/10.4319/lo.1975.20.6.0988, 1975.

Landais, A., Lathiere, J., Barkan, E., and Luz, B.: Reconsidering the change in global biosphere productivity between the Last Glacial Maximum and present day from the triple oxygen isotopic composition of air trapped in ice cores, Global Biogeochemical Cycles, 21, 2006GB002 739, https://doi.org/10.1029/2006GB002739, 2007.

Levine, N. M., Bender, M. L., and Doney, S. C.: The $\delta^{18}O$ of dissolved O_2 as a tracer of mixing and respiration in the mesopelagic ocean, Global Biogeochemical Cycles, 23, 2007GB003 162, https://doi.org/10.1029/2007GB003162, 2009.

Li, B., Hu, H., Berelson, W. M., Adkins, J. F., and Yeung, L. Y.: On the Use of Dissolved Oxygen Isotopologues as Biogeochemical Tracers in the Northeast Pacific Ocean, JGR Oceans, 127, e2022JC018 617, https://doi.org/10.1029/2022JC018617, 2022.

Loulergue, L., Schilt, A., Spahni, R., Masson-Delmotte, V., Blunier, T., Lemieux, B., Barnola, J.-M., Raynaud, D., Stocker, T. F., and Chappellaz, J.: Orbital and millennial-scale features of atmospheric CH4 over the past 800,000 years, Nature, 453, 383–386, https://doi.org/10.1038/nature06950, publisher: Nature Publishing Group, 2008.

Luz, B. and Barkan, E.: Assessment of Oceanic Productivity with the Triple-Isotope Composition of Dissolved Oxygen, Science, 288, 2028–2031, https://doi.org/10.1126/science.288.5473.2028, 2000.

Luz, B. and Barkan, E.: The isotopic ratios 17O/16O and 18O/16O in molecular oxygen and their significance in biogeochemistry, Geochimica et Cosmochimica Acta, 69, 1099–1110, https://doi.org/10.1016/j.gca.2004.09.001, 2005.

Luz, B. and Barkan, E.: Net and gross oxygen production from O2/Ar, 17O/16O and 18O/16O ratios, Aquatic Microbial Ecology, 56, 133–145, https://doi.org/10.3354/ame01296, 2009.

Luz, B., Barkan, E., Bender, M. L., Thiemens, M. H., and Boering, K. A.: Triple-isotope composition of atmospheric oxygen as a tracer of biosphere productivity, Nature, 400, 547–550, https://doi.org/10.1038/22987, 1999.

Marcus, R. A.: Theory of mass-independent fractionation of isotopes, phase space accessibility, and a role of isotopic symmetry, Proc. Natl. Acad. Sci. U.S.A., 110, 17 703–17 707, https://doi.org/10.1073/pnas.1213080110, 2013.

Marra, J.: Approaches to the Measurement of Plankton Production, in: Phytoplankton Productivity, edited by Williams, P. J. L. B., Thomas, D. N., and Reynolds, C. S., pp. 78–108, Wiley, 1 edn., ISBN 978-0-632-05711-5 978-0-470-99520-4, https://doi.org/10.1002/9780470995204.ch4, 2002.

Miller, M. F.: Isotopic fractionation and the quantification of 17O anomalies in the oxygen three-isotope system: an appraisal and geochemical significance, 2002.

Munro, D. R., Quay, P. D., Juranek, L. W., and Goericke, R.: Biological production rates off the Southern California coast estimated from triple O_2 isotopes and O_2 : Ar gas ratios, Limnology & Oceanography, 58, 1312–1328, https://doi.org/10.4319/lo.2013.58.4.1312, 2013.

Musan, I., Gildor, H., Barkan, E., Smethie, W. M., and Luz, B.: Evidence From Dissolved O_2 Isotopes in North Atlantic Deep Water for a Recent Climatic Shift, Geophysical Research Letters, 50, e2022GL100 489, https://doi.org/10.1029/2022GL100489, 2023.

Nicholson, D., Stanley, R. H. R., and Doney, S. C.: The triple oxygen isotope tracer of primary productivity in a dynamic ocean model, Global Biogeochemical Cycles, 28, 538–552, https://doi.org/10.1002/2013GB004704, 2014.

https://doi.org/10.5194/egusphere-2025-5230
Preprint. Discussion started: 21 January 2026

Nicholson, D. P., Stanley, R. H. R., Barkan, E., Karl, D. M., Luz, B., Quay, P. D., and Doney, S. C.: Evaluating triple oxygen isotope estimates of gross primary production at the Hawaii Ocean Time-series and Bermuda Atlantic Time-series Study sites, J. Geophys. Res., 117, 2010JC006 856, https://doi.org/10.1029/2010JC006856, 2012.

Opsteegh, J. D., Haarsma, R. J., Selten, F. M., and Kattenberg, A.: ECBILT: a dynamic alternative to mixed boundary conditions in ocean models, Tellus A: Dynamic Meteorology and Oceanography, 50, 348, https://doi.org/10.3402/tellusa.v50i3.14524, 1998.

Palevsky, H. I., Quay, P. D., Lockwood, D. E., and Nicholson, D. P.: The annual cycle of gross primary production, net community production, and export efficiency across the North Pacific Ocean, Global Biogeochemical Cycles, 30, 361–380, https://doi.org/10.1002/2015GB005318, 2016.

Quay, P. D., Emerson, S., Wilbur, D. O., Stump, C., and Knox, M.: The $\delta^{18}O$ of dissolved O_2 in the surface waters of the subarctic Pacific: A tracer of biological productivity, Journal of Geophysical Research: Oceans, 98, 8447–8458, https://doi.org/10.1029/92JC03017, _eprint: https://onlinelibrary.wiley.com/doi/pdf/10.1029/92JC03017, 1993.

Quay, P. D., Wilbur, D. ., Richey, J. E., Devol, A. H., Benner, R., and Forsberg, B. R.: The 18O:16O of dissolved oxygen in rivers and lakes in the Amazon Basin: Determining the ratio of respiration to photosynthesis rates in freshwaters, Limnol. Oceanogr., 40, 718–729, https://doi.org/10.4319/lo.1995.40.4.0718, 1995.

Reagan, J. R., Garcia, H. E., Boyer, T. P., Baranova, O. K., Bouchard, C., Cross, S. L., Dukhovskoy, D., Grodsky, A., Locarnini, R. A., Mishonov, A. V., Paver, C. R., Seidov, D., and Wang, Z.: World Ocean Atlas 2023: Product Documentation, https://repository.library.noaa.gov/view/noaa/70581, 2023.

Reuer, M. K., Barnett, B. A., Bender, M. L., Falkowski, P. G., and Hendricks, M. B.: New estimates of Southern Ocean biological production rates from O2/Ar ratios and the triple isotope composition of O2, Deep Sea Research Part I: Oceanographic Research Papers, 54, 951–974, https://doi.org/10.1016/j.dsr.2007.02.007, 2007.

Reutenauer, C., Landais, A., Blunier, T., Bréant, C., Kageyama, M., Woillez, M.-N., Risi, C., Mariotti, V., and Braconnot, P.: Quantifying molecular oxygen isotope variations during a Heinrich stadial, Clim. Past, 11, 1527–1551, https://doi.org/10.5194/cp-11-1527-2015, 2015.

Roche, D. M., Dokken, T. M., Goosse, H., Renssen, H., and Weber, S. L.: Climate of the Last Glacial Maximum: sensitivity studies and model-data comparison with the LOVECLIM coupled model, Clim. Past, 3, 205–224, https://doi.org/https://doi.org/10.5194/cp-3-205-2007, 2007.

Sarma, V. V. S. S., Abe, O., and Saino, T.: Spatial variations in time-integrated plankton metabolic rates in Sagami Bay using triple oxygen isotopes and O2:Ar ratios, Limnology and Oceanography, 53, 1776–1783, https://doi.org/10.4319/lo.2008.53.5.1776, _eprint: https://aslopubs.onlinelibrary.wiley.com/doi/pdf/10.4319/lo.2008.53.5.1776, 2008.

Schilt, A., Baumgartner, M., Blunier, T., Schwander, J., Spahni, R., Fischer, H., and Stocker, T. F.: Glacial–interglacial and millennial-scale variations in the atmospheric nitrous oxide concentration during the last 800,000 years, Quaternary Science Reviews, 29, 182–192, https://doi.org/10.1016/j.quascirev.2009.03.011, 2010.

Six, K. D. and Maier-Reimer, E.: Effects of plankton dynamics on seasonal carbon fluxes in an ocean general circulation model, Global Biogeochemical Cycles, 10, 559–583, https://doi.org/10.1029/96GB02561, 1996.

Stanley, R. H. R., Sandwith, Z. O., and Williams, W. J.: Rates of summertime biological productivity in the Beaufort Gyre: A comparison between the low and record-low ice conditions of August 2011 and 2012, Journal of Marine Systems, 147, 29–44, https://doi.org/10.1016/j.jmarsys.2014.04.006, 2015.

https://doi.org/10.5194/egusphere-2025-5230
Preprint. Discussion started: 21 January 2026

Sutherland, K. M., Johnston, D. T., Hemingway, J. D., Wankel, S. D., and Ward, C. P.: Revised microbial and photochemical triple-oxygen isotope effects improve marine gross oxygen production estimates, PNAS Nexus, 1, pgac233, https://doi.org/10.1093/pnasnexus/pgac233, 2022.

Thiemens, M. H., Jackson, T., Mauersberger, K., Schueler, B., and Morton, J.: Oxygen isotope fractionation in stratospheric CO2, Geophysical Research Letters, 18, 669–672, https://doi.org/10.1029/91GL00121, _eprint: https://agupubs.onlinelibrary.wiley.com/doi/pdf/10.1029/91GL00121, 1991.

Wanninkhof, R.: Relationship between wind speed and gas exchange over the ocean, J. Geophys. Res., 97, 7373–7382, https://doi.org/10.1029/92JC00188, 1992.

Westberry, T., Behrenfeld, M. J., Siegel, D. A., and Boss, E.: Carbon-based primary productivity modeling with vertically resolved photoacclimation, Global Biogeochemical Cycles, 22, 2007GB003 078, https://doi.org/10.1029/2007GB003078, 2008.

White, A., Karl, D., and Fujieki, L.: Primary productivity measurements for the Hawaii Ocean Time-Series (HOT) program from October 1988 to December 2023 at Station ALOHA., https://doi.org/10.26008/1912/bco-dmo.737163.4, 2025.

Wurgaft, E., Musan, I., Rivlin, T., and Luz, B.: Weak isotopic fractionation of dissolved O_2 during community respiration, Limnology & Oceanography, 67, 1794–1804, https://doi.org/10.1002/lno.12167, 2022.

Yeung, L. Y., Berelson, W. M., Young, E. D., Prokopenko, M. G., Rollins, N., Coles, V. J., Montoya, J. P., Carpenter, E. J., Steinberg, D. K., Foster, R. A., Capone, D. G., and Yager, P. L.: Impact of diatom-diazotroph associations on carbon export in the Amazon River plume, Geophysical Research Letters, 39, https://doi.org/10.1029/2012GL053356, _eprint: https://agupubs.onlinelibrary.wiley.com/doi/pdf/10.1029/2012GL053356, 2012.

Yung, Y. L., DeMore, W. B., and Pinto, J. P.: Isotopic exchange between carbon dioxide and ozone via $O(^1D)$ in the stratosphere, Geophysical Research Letters, 18, 13–16, https://doi.org/10.1029/90GL02478, 1991.